Simulation of aeolian sand saltation with rotational motion

Ning Huang,[1] Cong Wang,[1] and Xiying Pan[1]

Received 30 November 2009; revised 8 July 2010; accepted 14 July 2010; published 24 November 2010.

[1] In this work, we propose a theoretical model based on the distribution functions of initial liftoff velocity and angular velocity of sand grains to describe a sand saltation process in which both wind field–sand grain coupling and the Magnus force experienced by saltating sand grains have been incorporated. The computation results showed that the Magnus force had significant effects on sand grain saltation. In particular, when the Magnus force was incorporated, the calculated sand transport fluxes and sand transport rate per unit width were closer to the experimental value than when this force was excluded. The sand transport flux is enhanced because the Magnus force owing to particle rotation causes the particles to have higher and longer trajectories, so the particles can get more speed and energy from the wind, which leads to a larger sand transport flux. In addition, it was found that when taking the Magnus force into account, the probability density of the impact velocity and angular velocity of saltating sand grains followed an exponential distribution and a unimodal asymmetric distribution, respectively. Moreover, the sand energy flux increased with the height above the sand surface until the energy flux reached its maximum and then decreased. Furthermore, the energy flux near the ground surface decreased as the grain diameter increased, but beyond a specific height the energy flux increased with the grain diameter. Finally, for the same sand grain diameter, the energy flux increased with the friction velocity.

Citation: Huang, N., C. Wang, and X. Pan (2010), Simulation of aeolian sand saltation with rotational motion, *J. Geophys. Res.*, *115*, D22211, doi:10.1029/2009JD013593.

1. Introduction

[2] There are three kinds of principal sand particle movements in typical aeolian sand transport, i.e., creeping, saltation, and suspension. Of these, saltation is predominant, with saltating sand grains accounting for about 75% of the total sand transported [*Bagnold*, 1941; *Shao*, 2000]. Creeping and suspension are primarily initiated by the impact of particles in saltation [*Anderson et al.*, 1991a; *Bagnold*, 1941; *Shao*, 2000; *Kok and Renno*, 2008]. The understanding of aeolian sand movement has been advanced considerably in the past few years, largely because of the development of numerical simulations of saltation, which can provide significant insights on the essential underlying physical processes [*Anderson et al.*, 1991a; *Huang et al.*, 2006; *Kok and Renno*, 2008, 2009]. In particular, many studies have been published recently dealing with models of aeolian sand transport and numerical simulation of the macroscopic physical quantities characterizing aeolian sand movement, such as the height profile of sand transport flux, sand transport rate per unit width, and the wind velocity profile within the saltation layer. However, the currently available theoretical models are still far from being able to reliably and quantitatively predict the sand transport rate [*Anderson et al.*, 1991a], although some significant improvements have been achieved [for example, *Bo and Zheng*, 2007; *Kok and Renno*, 2009]. The difficulty is probably due to the oversimplification of current theoretical models describing aeolian sand transport process. For example, in simulations conducted by *Anderson and Haff* [1988] and *Anderson et al.* [1991b], the wind field was assumed to be steady; that is, the time variation of the wind field had not been included. Moreover, the Magnus force due to particle spin has been neglected in almost all theoretical models, although a recent model by *Kok and Renno* [2009] did include the Magnus force, and it was shown that particle spin indeed affects particle trajectories.

[3] In fact, various rotational motions are ubiquitous in sand grain movements in aeolian sand transport, whether in rolling and sliding on the ground or in saltation and suspension [*Zheng et al.*, 2006; *Zou et al.*, 2007]. The rotational motion of saltating sand grains has been reported by most authors, and the rotational speed of saltating particles has been observed in a range of 220 ~ 1000 rev s^{-1} [*Bagnold*, 1941; *Chepil and Woodruff*, 1963; *Zou et al.*, 2007]. *White and Schultz* [1977] proposed that the Magnus force can significantly influence sand saltation and, in particular, that the sand saltation height can be increased by about 20%. Because of the significant effect of the Magnus force on sand saltation, it is reasonable to expect that the Magnus force could affect the sand transport rate too. In a numerical simulation study of saltation conducted by *Huang and*

[1]Key Laboratory of Mechanics on Disaster and Environment in Western China, Ministry of Education, Department of Mechanics, Lanzhou University, Lanzhou, China.

0148-0227/10/2009JD013593

Zheng [2003] at liftoff angular velocities of 200, 400, and 600 rev s^{-1}, it was found that the Magnus force can significantly affect the trajectory of saltating sand grains and that the effects increased with the magnitude of the liftoff angular velocity. In a similar study, *Zou et al.* [2007] investigated the effects of the Magnus force on the maximum saltation height and saltation length of sand grains. However, it is almost impossible that all sand grains will possess the identical liftoff velocity or identical liftoff angular velocity. Therefore, the studies conducted by *White and Schultz* [1977], *Huang and Zheng* [2003], and *Zou et al.* [2007] can only illuminate the Magnus force effects on the trajectory of a single saltating sand grain. Thus, they cannot reveal the effects of the Magnus force on macroscopic physical quantities that characterize the global aeolian sand transport process, such as the height profile of sand transport flux, the sand transport rate per unit width per unit time, and the wind velocity profile within saltation layer. Therefore, these studies failed to accurately predict these macroscopic physical quantities.

[4] In addition, the study of the energy of saltating sand grains is particularly important. It is the huge amount of energy that sand grains gain from winds that predominates in aeolian sand disasters, such as crop and vegetation damage, destruction of buildings caused by aeolian sand flow, and drastic soil erosion resulting from the impact of aeolian sand flow on the ground surface. Therefore, a sufficiently accurate prediction of the energy of aeolian sand flow is crucial in evaluating the extent of damage caused by aeolian sand flow.

[5] While the height profile of aeolian sand flow energy has been analyzed by several authors, the energy of saltating particles cannot be accurately measured in most situations because of the small size of sand grains as well as the large relative velocities, which makes the measurements of mass movements very difficult [*Gillette and Stockton*, 1986; *Anderson and Hallet*, 1986; *Zou et al.*, 2001; *Rasmussen and Sorensen*, 2008]. On the other hand, although the height variation of aeolian sand flow energy has been determined by *Anderson and Hallet* [1986] through numerical simulation, these result cannot be used to accurately describe the energy distribution in real-world aeolian sand flow because of the crudeness of model used, and especially because the model does not include the Magnus force; that is, it neglects the contribution of sand grain rotation to the energy.

[6] In this work, we propose a theoretical model based on the distribution function of initial liftoff velocity [*Huang et al.*, 2006] and angular velocity [*Zheng et al.*, 2006] of sand grains to describe a sand saltation process in which wind field–sand grain coupling and the Magnus effect have been included. The effects of the Magnus force on sand grain saltation and the height variation of sand grain energy have been studied in detail using numerical simulation; in addition, the distribution of impact velocity and angular velocity of saltating sand grains have also been determined.

2. Theoretical Model and Governing Equations

[7] Consider a two-dimensional steady state aeolian sand flow on an infinite sand plane at $y = 0$, in which the wind blows along the x axis with a friction velocity u_*. The sand grains are spherical and have the same diameter.

2.1. Sand Grain and Wind Field Governing Equations

[8] The governing equations of sand grains moving along the x-y plane and subject to gravity, drag force, and the Magnus force are as follows [*White and Schultz*, 1977; *Zheng et al.*, 2006]:

$$m_p\frac{d^2x}{dt^2} = -\frac{\rho\pi D_p^2}{8}\left(\frac{24\nu}{D_p\sqrt{(\dot{x}-u)^2+\dot{y}^2}} + \frac{6}{1+\sqrt{D_p\sqrt{(\dot{x}-u)^2+\dot{y}^2}/\nu}} + 0.4\right) \times (\dot{x}-u)\sqrt{(\dot{x}-u)^2+\dot{y}^2} + \frac{1}{8}\pi\rho D_p^3\dot{y}\left(\dot{\theta}-\frac{1}{2}\frac{du}{dy}\right), \quad (1)$$

$$m_p\frac{d^2y}{dt^2} = -\frac{\rho\pi D_p^2}{8}\left(\frac{24\nu}{D_p\sqrt{(\dot{x}-u)^2+\dot{y}^2}} + \frac{6}{1+\sqrt{D_p\sqrt{(\dot{x}-u)^2+\dot{y}^2}/\nu}} + 0.4\right) \times \dot{y}\sqrt{(\dot{x}-u)^2+\dot{y}^2} - m_p g + \frac{1}{8}\pi\rho D_p^3(\dot{x}-u)\left(\dot{\theta}-\frac{1}{2}\frac{du}{dy}\right), \quad (2)$$

$$m_p\frac{pd^2\theta}{d^2t} = 10\pi\mu D_p\left(\dot{\theta}-\frac{1}{2}\frac{du}{dy}\right), \quad (3)$$

in which x and y are the position coordinate of sand grain in x-y plane; m_p is the sand grain mass; t is time; D_p is sand grain diameter; v is the air kinematic viscosity; $\dot{x}$ and $\dot{y}$ are the sand grain velocity along the x and y axis, respectively; u is the wind velocity; θ is the sand grain rotation angle; $\dot{\theta}$ is sand grain rotation angular velocity, g is the acceleration of gravity; and μ is the air viscosity.

[9] The Navier-Stokes equations of a two-dimensional steady airflow over an infinite flat plane can be significantly simplified by using mixing length theory [*Ungar and Haff*, 1987; *Werner*, 1990; *Anderson et al.*, 1991b], and the equation along the x axis can be written as

$$\frac{du}{dy} = \frac{1}{ky}\left[\frac{\rho u_*^2 - \int_y^{y_{max}} F_x(y)dy}{\rho}\right]^{\frac{1}{2}}, \quad (4)$$

in which u_* is the friction velocity, y_{max} represents the maximum height that can be reached by saltating sand grains and $F_x(y)$ is the friction force per unit volume exerted by sand grains upon the airflow. If both u_* and $F_x(y)$ are known, $u(y)$, the height profile of the wind velocity within the saltation layer, or more precisely, the wind field after incorporating the sand grain counteractions, can be immediately obtained from equation (4).

2.2. Liftoff Velocity and Angular Velocity Distribution of Sand Grains

[10] According to *Huang et al.* [2006], the sand grain liftoff velocity distribution can be expressed as an exponential function of initial velocity v_0:

$$p(v_0) = \left(-0.247 + 0.366e^{u*/0.747}\right)^{-1} \cdot \exp\left(-\frac{v_0}{-0.247 + 0.366e^{u*/0.747}}\right). \quad (5)$$

[11] The sand grain liftoff angular velocity distribution is related to the sand grain diameter and wind speed [*Zheng et al.*, 2006] and can be represented by

$$f(\dot{\theta}_0) = af(\dot{\theta}_A) + bf(\dot{\theta}_B), \quad (6)$$

in which $\dot{\theta}_0$ is the liftoff angular velocity of sand grains; $\dot{\theta}_A$ is the liftoff angular velocity of rebounding sand grains; $\dot{\theta}_B$ is the liftoff angular velocity of splashing sand grains; and $f(\dot{\theta}_0)$, $f(\dot{\theta}_A)$, and $f(\dot{\theta}_B)$ are the distribution function of $\dot{\theta}_0$, $\dot{\theta}_A$ and $\dot{\theta}_B$, respectively. Coefficients a and b are the rebounding and splashing coefficient, respectively; both can be determined from experiments and change with sand grain diameter and wind speed. Functions $f(\dot{\theta}_A)$ and $f(\dot{\theta}_B)$ are dependent on wind velocity and particle diameter and are given by equations (7) and (8) [*Zheng et al.*, 2006].

$$f(\dot{\theta}_A) = \int\int\int\int \cdot \frac{2R_A f_{V_A} f_{\theta_0} f_{V_B} \left|9 + 4R_A^3[1 + \sin(\alpha + \beta)][2 - \sin(\alpha + \beta)]/R_B^3\right|}{|4(1 + k)[1 + \sin(\alpha + \beta)]|} \cdot d\beta d\theta_0 d\alpha dV_A. \quad (7)$$

$$f(\dot{\theta}_B) = \int\int\int\int \cdot \frac{R_B f_{V_A} f_{\theta_0} f_{V_B} \left|9 + 4R_A^3[1 + \sin(\alpha + \beta)][2 - \sin(\alpha + \beta)]/R_B^3\right|}{3(1 + k)} \cdot d\beta d\theta_0 d\alpha dV_A. \quad (8)$$

2.3. Calculation of Frictional Force Exerted by Saltating Sand Grains on the Wind

[13] The force exerted by the wind upon sand grains is actually the reaction force of that exerted by sand grains upon the wind. Consequently, both have the same magnitude but opposite direction. The frictional force per unit volume exerted by sand grains upon the wind can be calculated by $F_x(y) = m_p a_x(y)$ and can be written as [*Anderson et al.*, 1991b; *Huang et al.*, 2006]

$$F_x(y) = -sm_p \int\int p(v_0) f(\dot{\theta}_0) \left[\frac{a_{x\uparrow}}{|\dot{y}_{\uparrow(y)}|} + \frac{a_{x\downarrow}}{|\dot{y}_{\downarrow(y)}|}\right] dv_0 d\dot{\theta}_0, \quad (9)$$

in which s is the number of sand grains ejected from the sand bed per unit area and per unit time and the subscripts $\uparrow$ and $\downarrow$ indicate the ascending and descending stage, respectively.

2.4. Calculation of Sand Transport Rate per Unit Width

[14] Under the circumstances that the Magnus force, i.e., the rotation of sand grains, is neglected, the sand transport rate per unit width at height y can be calculated by [*Anderson et al.*, 1991b; *Huang et al.*, 2006]

$$q(y) = m_p s \int_{v_{0\min}}^{v_{0\max}} \left[\frac{\dot{x}_\uparrow(y, v_0)}{\dot{y}_\uparrow(y, v_0)} - \frac{\dot{x}_\downarrow(y, v_0)}{\dot{y}_\downarrow(y, v_0)}\right] p(v_0) dv_0, \quad (10)$$

where $v_{0\min}$ and $v_{0\max}$ represent the minimal and maximal initial velocity required for saltating sand grains to reach height y. In particular, the sand transport rate per unit width can be obtained by integrating equation (10) from $y = 0$ (bed surface) to infinity:

$$Q = m_p s \int_0^\infty \int_{v_{0\min}}^{v_{0\max}} \left[\frac{\dot{x}_\uparrow(y, v_0)}{\dot{y}_\uparrow(y, v_0)} - \frac{\dot{x}_\downarrow(y, v_0)}{\dot{y}_\downarrow(y, v_0)}\right] p(v_0) dv_0 dy. \quad (11)$$

On the other hand, after incorporating the Magnus force, the flux of sand grains M lifting off from the bed surface with an initial velocity and angular velocity v_0 and $\dot{\theta}_0$, respectively, can be expressed by

$$M = m_p s p(v_0) f(\dot{\theta}_0) dv_0 d\dot{\theta}_0. \quad (12)$$

[15] Consequently, the sand transport rate at height y when the Magnus force has been included can be obtained from equations (11) and (12):

$$q(y) = m_p s \int_{\dot{\theta}_{0\min}}^{\dot{\theta}_{0\max}} \int_{v_{0\min}}^{v_{0\max}} \left[\frac{\dot{x}_\uparrow(y, v_0, \dot{\theta}_0)}{\dot{y}_\uparrow(y, v_0, \dot{\theta}_0)} - \frac{\dot{x}_\downarrow(y, v_0, \dot{\theta}_0)}{\dot{y}_\downarrow(y, v_0, \dot{\theta}_0)}\right] \cdot p(v_0) f(\dot{\theta}_0) dv_0 d\dot{\theta}_0, \quad (13)$$

in which $\dot{\theta}_{0\min}$ and $\dot{\theta}_{0\max}$ are the minimal and maximal rotational angular velocity of sand grains, respectively. The sand transport rate per unit width can be calculated by integrating equation (13) from $y = 0$ to infinity:

$$Q = m_p s \int_0^\infty \int_{\dot{\theta}_{0\min}}^{\dot{\theta}_{0\max}} \int_{v_{0\min}}^{v_{0\max}} \left[\frac{\dot{x}_\uparrow(y, v_0, \dot{\theta}_0)}{\dot{y}_\uparrow(y, v_0, \dot{\theta}_0)} - \frac{\dot{x}_\downarrow(y, v_0, \dot{\theta}_0)}{\dot{y}_\downarrow(y, v_0, \dot{\theta}_0)}\right] \cdot p(v_0) f(\dot{\theta}_0) dv_0 d\dot{\theta}_0 dy. \quad (14)$$

2.5. Calculation of Energy Flux

[16] As shown by *Zou et al.* [2001], the gravitational potential energy of sand grains can be neglected compared to their kinetic energy. Therefore, only sand grain kinetic energy has been considered here. Particularly, the energy flux at height y, when neglecting the Magnus force or sand grain rotation, can be expressed by:

$$E(y) = \frac{1}{2} m_p s \int_{v_{0\min}}^{v_{0\max}} \cdot \left[\frac{\dot{x}_\uparrow(y, v_0)\left(\dot{x}_\uparrow^2(y, v_0) + \dot{y}_\uparrow^2(y, v_0)\right)}{\dot{y}_\uparrow(y, v_0)} - \frac{\dot{x}_\downarrow(y, v_0)\left(\dot{x}_\downarrow^2(y, v_0) + \dot{y}_\downarrow^2(y, v_0)\right)}{\dot{y}_\downarrow(y, v_0)}\right] \cdot p(v_0) dv_0. \quad (15)$$

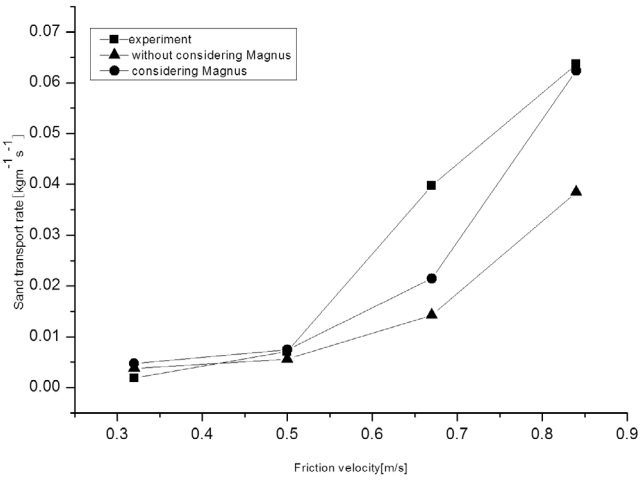

Figure 1. The calculated 0.228 mm sand transport rate per unit width, with and without the Magnus force, and the corresponding experimental results [*Huang et al.*, 2006].

On the other hand, when considering the Magnus force, both the rotational and translational kinetic energy of sand grains must be taken into account.

[17] Finally, the energy flux at height y, after incorporating the Magnus force, can be calculated by

$$E(y) = \frac{1}{2} m_p s \int_{\dot{\theta}_{0\min}}^{\dot{\theta}_{0\max}} \int_{v_{0\min}}^{v_{0\max}} \cdot \left[\frac{\dot{x}_\uparrow(y, v_0, \dot{\theta}_0)\left(\dot{x}_\uparrow(y, v_0, \dot{\theta}_0)^2 + \dot{y}_\uparrow(y, v_0, \dot{\theta}_0)^2 + \frac{1}{10}\dot{\theta}_\uparrow^2(y, v_0, \dot{\theta}_0) D_p^2\right)}{\dot{y}_\uparrow(y, v_0, \dot{\theta}_0)} - \frac{\dot{x}_\downarrow(y, v_0, \dot{\theta}_0)\left(\dot{x}_\downarrow(y, v_0, \dot{\theta}_0)^2 + \dot{y}_\downarrow(y, v_0, \dot{\theta}_0)^2 + \frac{1}{10}\dot{\theta}_\downarrow^2(y, v_0, \dot{\theta}_0) D_p^2\right)}{\dot{y}_\downarrow(y, v_0, \dot{\theta}_0)} \right] \cdot p(v_0) f(\dot{\theta}_0) dv_0 d\dot{\theta}_0. \quad (16)$$

3. Calculation Procedure and a Description of Experiments

3.1. Initial Conditions

[18] The initial conditions of sand grain governing equations after incorporating the Magnus force are:

$$\pm = 0: \; x = 0, y = 0, \theta = 0; \qquad \dot{x} = 0, \dot{y} = v_0, \dot{\theta} = \dot{\theta}_0. \quad (17)$$

The height profile of the initial wind speed can be described by a logarithmic function,

$$u = \frac{u_*}{k} \ln\left(\frac{y}{y_0}\right), \quad (18)$$

in which the surface roughness y_0 is set to be $D_p/30$ [*Bagnold*, 1941]. The friction wind velocity u_* is calculated on the basis of the axial wind speed u_{in} that is measured experimentally by [*Zhou et al.*, 2002]:

$$u_* = (u_{in} - 4.3)/11.5. \quad (19)$$

On the basis of our experimental observations, the threshold velocity of this sand bed in the wind tunnel is about 7 m s^{-1}; thus, its fluid friction velocity threshold is calculated as 0.23 m s^{-1} by equation (19).

[19] *Owen* [1964] proposed a hypothesis that when the windblown sand flux attains a steady state, the shear stress exerted by wind on the surface should be just sufficient to maintain the sand-strewn surface in a mobile state because of the reaction force of particles on the wind. Many scientists [e.g., *Anderson and Haff*, 1988; *Anderson et al.*, 1991a; *Kok and Renno*, 2009] have cited this hypothesis, and it is used as the criterion for the steady state of windblown sand movement in this paper. *Bagnold* [1941] found that the threshold of the impact friction velocity is about 80% of the threshold of the fluid friction velocity. Further, the threshold of the impact friction velocity is accordingly given as $u_{it*} = 0.8 \times 0.23 = 0.184$ m s^{-1}, and the density of air is 1.22 kg m^{-3}. Therefore the threshold of impact shear stress is

$$\tau_{ti} = \rho u_{it*}^2 = 1.22 \times 0.184^2 = 0.043 \text{ N m}^{-2}. \quad (20)$$

In addition, the diameter of sand grains simulated is 0.228 mm, 0.25 mm, 0.35 mm, and 0.45 mm. The density of sand grains and air are 2650 kg m^{-3} and 1.22 kg m^{-3}, respectively. The air kinematic viscosity v and viscosity μ are 1.5×10^{-5} m^2 s^{-1} and 1.8×10^{-5} kg m^{-1} s^{-1}, respectively.

3.2. Calculation Procedure

[20] The following are the steps used in the calculation.

[21] 1. The value of parameters D_p, τ_{ti} and u_{in} are entered, the initial friction velocity is calculated by substituting u_{in} into equation (19). The initial wind velocity profile $u^i(y)$(i = 1 here) is obtained by substituting u_* into equation (18).

[22] 2. The initial liftoff velocity distribution $p^i(v_0)$(i = 1) is calculated by equation (5). Then, the initial liftoff angular velocity $f^i(\dot{\theta}_0)$(i = 1) is obtained from equation (6).

[23] 3. The trajectories $x^i(t)$, $y^i(t)$, and $\theta^i(t)$ and the corresponding velocity and angular velocities $\dot{x}^i(t)$, $\dot{y}^i(t)$, and $\dot{\theta}^i(t)$ of saltating sand grains are calculated after substituting $u^i(y)$ into equations (1)–(3).

[24] 4. Substituting s, $p^i(v_0)$, $f^i(\dot{\theta}_0)$, $x^i(t)$, $y^i(t)$, $\theta^i(t)$, $\dot{x}^i(t)$, $\dot{y}^i(t)$, and $\dot{\theta}^i(t)$ into equation (9), the force exerted by sand grains upon the wind $F_x^i(y)$ is obtained.

[25] 5. Substituting $F_x^i(y)$ into equation (4), the wind velocity profile that includes the modification caused by saltating sand grains can be calculated. Steps 3–5 are repeated until the converged wind velocity profile $u^{i+1}(y)$ is obtained. The shear stress upon the sand surface exerted by the wind, τ^{i+1}, is subsequently calculated.

[26] 6. Depending on whether τ^{i+1} is larger or smaller than τ_{ti}, a larger or smaller s value is chosen and steps 2–5 are repeated until $|\tau^{i+1} - \tau_{ti}| \le 0.001$ N m^{-2}.

[27] 7. Substituting the value of s, $p^i(v_0)$, $f^i(\dot{\theta}_0)$, $x^i(t)$, $y^i(t)$, $\theta^i(t)$, $\dot{x}^i(t)$, $\dot{y}^i(t)$, and $\dot{\theta}^i(t)$ calculated in step 6 into equations (13) and (14), the sand transport flux and sand transport rate per unit width after incorporating the Magnus force can be determined. Similarly, substituting the value of

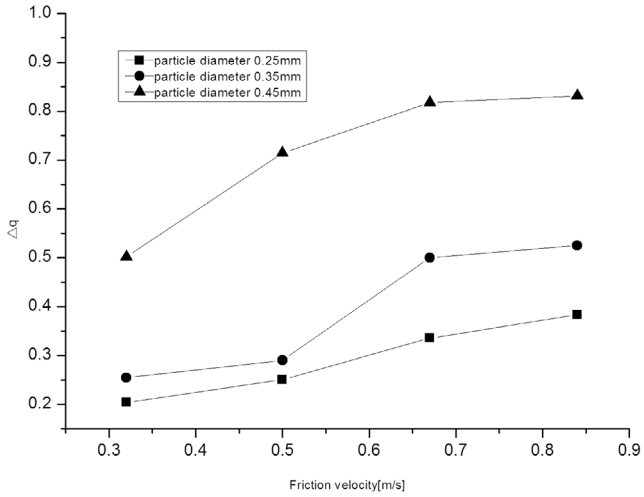

Figure 2. The relative difference between the sand transport rates per unit width calculated with and without the Magnus force versus the friction velocity.

s, $p^i(v_0)$, $f^i(\dot{\theta}_0)$, $x^i(t)$, $y^i(t)$, $\theta^i(t)$, $\dot{x}^i(t)$, $\dot{y}^i(t)$, and $\dot{\theta}^i(t)$ calculated in step 6 into equation (16), the energy flux after incorporating the Magnus force can be calculated at various heights.

3.3. Short Description of Experimental Observations

[28] In section 4, we use some experimental results to support our simulated results. Here we give a short description of how the actual observations of particle flux density profiles and particle energy profiles were obtained. To get the sand flux, saltating sand was collected by using a step-like sand collector [*Zhou et al.*, 2002; *Huang et al.*, 2006] that is 0.3 m high and 0.01 m wide, with 30 vertical square openings of 0.0001 m^2. By weighing the sand collected in each tube, one can obtain measurements of the sand flux through a 0.0001 m^2 opening at each 0.01 m above the sand surface beginning at 0.04 m above the sand surface. The mean distance from the sand surface to the edge of the lowest opening of the sand collector was 0.04 m. Thus, we obtained estimates of the sand flux at 30 different heights from 0.045 to 0.335 m. The collected sand samples were weighed using a Mettler PM480 with microgram

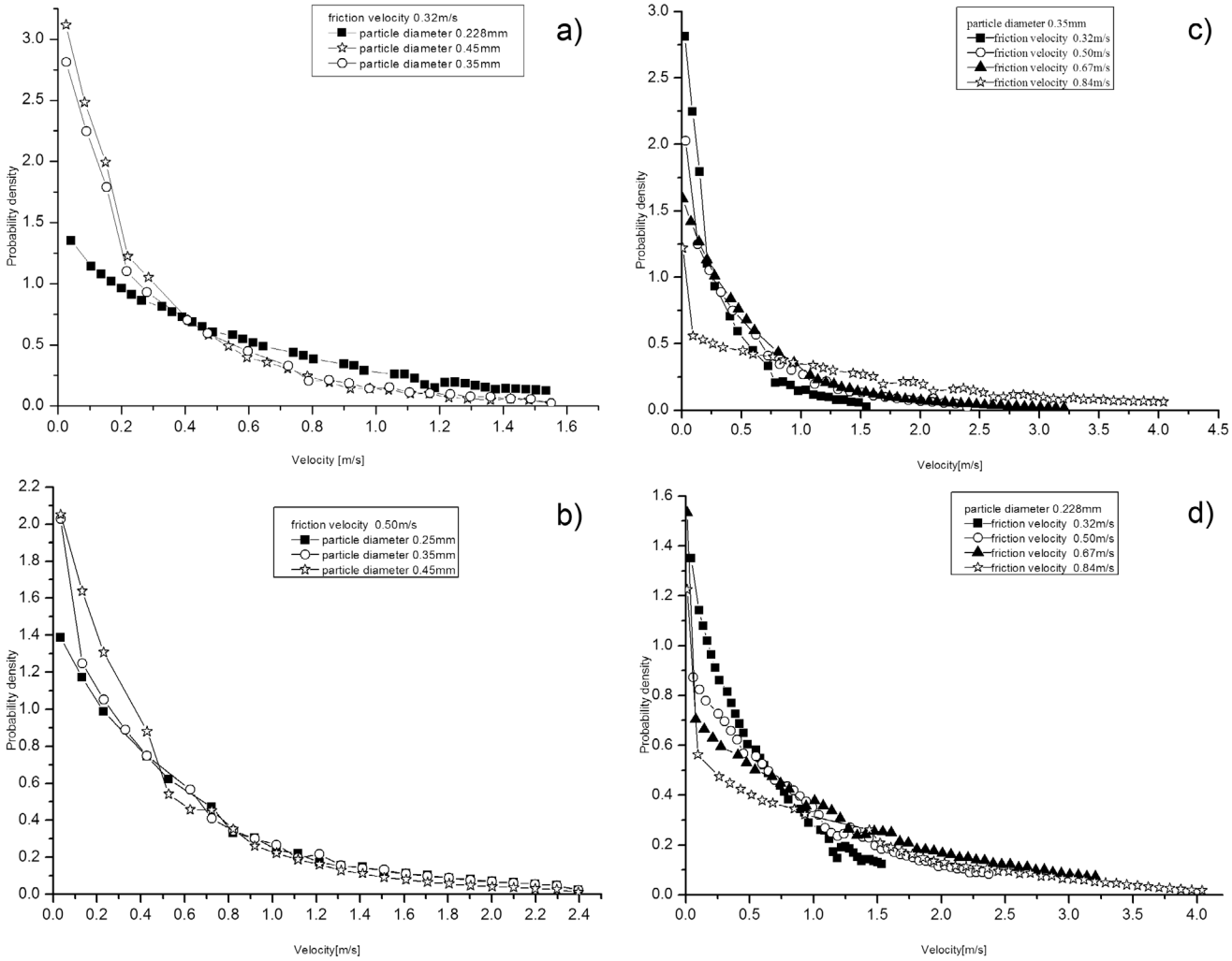

Figure 3. The simulated probability distribution of saltating sand grain impact velocity: (a) friction velocity 0.32 m s^{-1}, (b) friction velocity 0.50 m s^{-1}, (c) particle diameter 0.35 mm, and (d) particle diameter 0.228 mm.

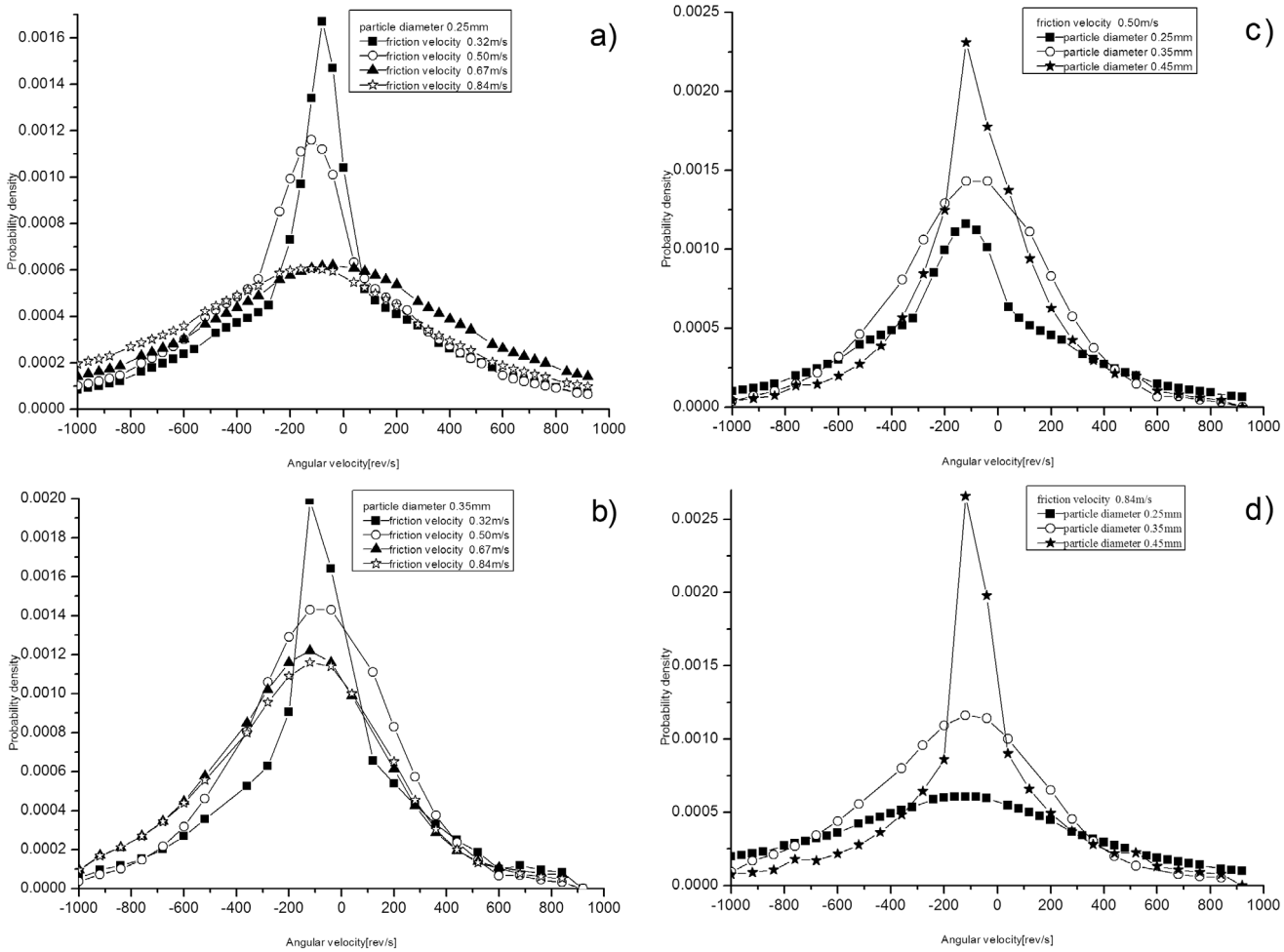

Figure 4. The simulated probability distribution of saltating sand grain impact angular velocity: (a) particle diameter 0.25 mm, (b) particle diameter 0.35 mm, (c) friction velocity 0.50 m s^{-1}, and (d) friction velocity 0.84 m s^{-1}.

precision. Dividing the sand mass collected in each tube by the area of its corresponding opening and the duration of the experiment yields the average horizontal sand flux at the center of each opening. Through fitting a set of experimental results of sand flux varying with height, one can obtain a formula for sand flux with the variable of height. The sand transport rate per unit width can be obtained through integrating the formula for sand flux with respect to the variable of height [*Zhou et al.*, 2002; *Huang et al.*, 2006].

[29] In the sand energy experiments, high-speed multiflash photography is used for studying the energy distribution of saltating grains within the boundary layer of a wind tunnel. Images of sand trajectories are obtained by a high-speed multiflash photographic technique. The velocity of each sand grain can be calculated by analyzing the images of its trajectory. Finally, energy distributions are obtained through the theorem of kinetic energy [*Zou et al.*, 2007].

4. Results and Discussion

[30] The sand transport rate has been calculated for various sand grain diameters and friction velocities under the circumstances that the Magnus force is incorporated or not. Figure 1 shows the calculated transport rate per unit width for a 0.228 mm sand grain at friction velocities of 0.32 m s^{-1}, 0.50 m s^{-1}, 0.67 m s^{-1}, and 0.84 m s^{-1} with and without the Magnus force, as well as the corresponding experimental results. As shown in Figure 1, the calculated transport rates per unit width with the Magnus force incorporated were closer to the experimental values than those calculated without incorporating the Magnus force. The sand transport rate is enhanced because the Magnus force owing to particle rotation causes particles to have higher and longer trajectories, so the particles can get more speed and energy from the wind, which leads to a larger sand transport flux. Additionally, the transport rates per unit width were found to increase with the friction velocity.

[31] The relative difference between the sand transport rate per unit width calculated with the Magnus force and without the Magnus force, i.e., $\Delta q = (q_1 - q_2)/q_1$, are plotted against the friction velocity in Figure 2 for sand grains of diameter 0.25 mm, 0.35 mm, and 0.45 mm, in which q_1 and q_2 are the sand transport rate per unit width with and without the Magnus force, respectively. As shown in Figure 2, the effects of the Magnus force were not obvious at small sand grain diameters but became significant as the sand grain

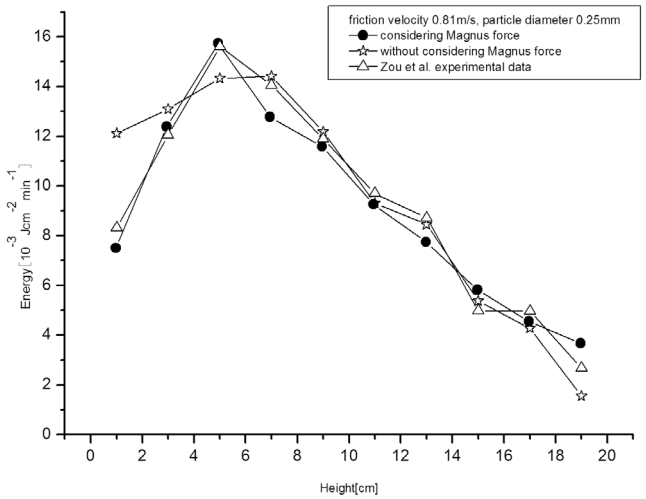

Figure 5. The height profile of energy flux with and without the Magnus force.

diameter increased. At higher diameters, the calculated sand transport rate per unit width with the Magnus force was obviously larger than the rate without the Magnus force, and their relative difference increased with friction velocity. Therefore, the effect of Magnus force on the sand transport rate cannot be ignored.

[32] The probability distributions of the sand grain impact velocity and angular velocity, as well as the distribution function of the initial liftoff velocity and angular velocity, are shown in Figures 3 and 4. As shown in Figure 3, the probability density of sand grain impact velocity still follows an exponential distribution even though the Magnus force is taken into account. In particular, for the same sand grain diameter, the probability density of the sand grain impact velocity decreases with the friction velocity when the impact velocities were rather small (near zero) but increased with the friction velocity after the impact velocity reached a specific value. On the contrary, at the same friction velocity, the probability density of the sand grain impact velocity increased with sand grain diameter when the impact velocities were rather small (near zero) but decreased with sand grain diameter after the impact velocity reached a specific value. The probability distribution of the impact speed is broader for smaller particles because the following behavior of smaller particles is better than larger particles in a wind field, and smaller particles are more easily accelerated by wind. When the wind velocity is small and close to the threshold, the possibilities of low impact velocity for particles of $d = 350$ μm and $d = 450$ μm are much higher than that for particles of $d = 228$ μm (Figure 3a). As wind velocity increases, the difference between $d = 250$ μm and $d = 350$ μm becomes smaller and the difference between $d = 350$ μm and $d = 450$ μm becomes clearer (Figure 3b).

[33] On the other hand, as shown in Figure 4, the probability density of the impact angular velocity of saltating sand grains was found to follow a unimodal asymmetric distribution. On the upper side of the topspin particle, it spins in the same direction as the fluid motion, and on the lower side of the particle it spins in the opposite direction to the fluid. Because the fluid velocity on the upper side of the topspin particle is relatively higher than that on the lower side of the particle, the overall effect of the wind on the particle will enhance its spin velocity. But for the backspin particle, the overall effect of the wind on the particle will be to diminish its spin velocity. This effect causes an asymmetry in the unimodal distribution of the particle rotation rate. From Figure 4 it can also be seen that for the same sand grain diameter, the probability distribution became more and more concentrated near the origin (angular velocity = 0) as the friction velocity decreased, while the probability density far away from the origin increased with the friction velocity. In contrast, for the same friction velocity, the probability density around the origin decreased as the sand grain diameter decreased, while the probability density far away from the origin increased.

[34] The calculated energy flux at various heights, as well as the corresponding experimental results [*Zou et al.*, 2001], are shown in Figure 5, in which the friction velocity of wind u_* and sand grain diameter D_p were fixed at 0.81 m s^{-1} and 0.25 mm, respectively. Specifically, as shown in Figure 5, the energy flux increased with the height until the energy

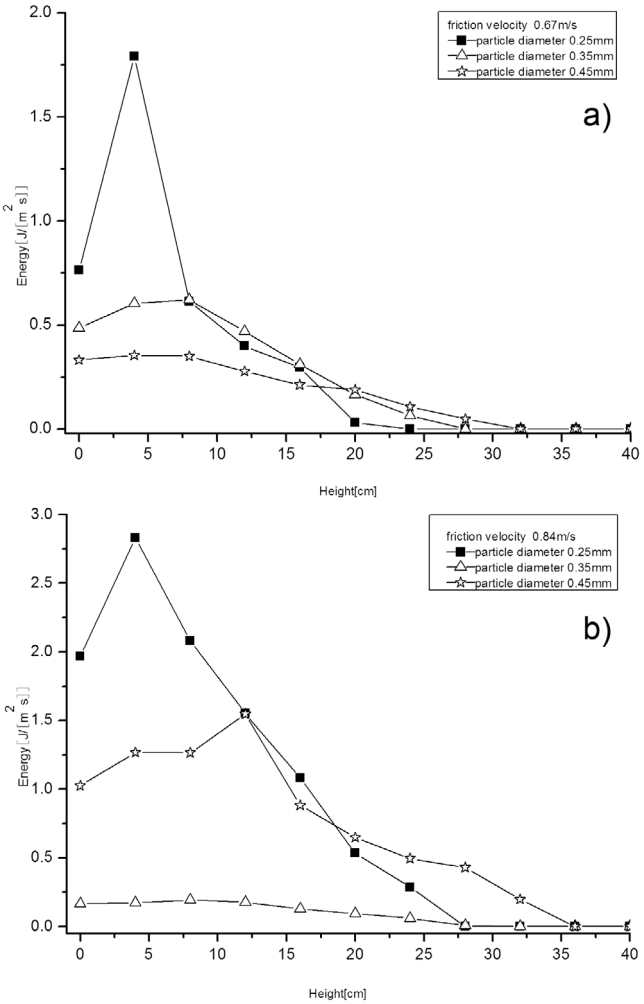

Figure 6. The simulated results of height profile of energy flux for various grain diameters: (a) friction velocity 0.67 m s^{-1} and (b) friction velocity 0.84 m s^{-1}.

flux reached its maximum, and then the energy flux began to decrease as the height increased. Meanwhile, the calculated energy fluxes with the Magnus force being included were closer to the experimental values than those without.

[35] The distributions of energy flux along the height at a fixed friction velocity were plotted in Figure 6 for various sand grain diameters. In particular, as shown in Figure 6, the energy flux decreased as grain diameter increased near the ground surface, but, in contrast, increased with grain diameter beyond a specific height. In addition, for the same grain diameter, the energy flux increased with friction velocity.

5. Conclusions

[36] In this work, we proposed a theoretical model based on the distribution function of initial liftoff velocity and angular velocity of sand grains to describe a sand saltation process in which both wind field–sand grain coupling and the Magnus force experienced by saltating sand grains have been incorporated. A series of numerical simulation studies have been conducted based on the proposed model. On the basis of the simulation results, we can conclude that:

[37] 1. The Magnus force exhibited significant effects on some macroscopic quantities that describe the saltation process in aeolian sand transport, such as the height profile of sand transport flux and the sand transport rate per unit width. In particular, the calculated results with the Magnus force incorporated were closer to the corresponding experimental value than those without.

[38] 2. The probability density of the impact velocity of saltating sand grains followed an exponential distribution, while the probability density of the corresponding impact angular velocity obeyed a unimodal asymmetrical distribution.

[39] 3. For the same grain diameter, the energy flux at the same height increased with wind speed, while at the same wind speed, the energy flux decreased with the height. The calculated energy fluxes with the Magnus force included were closer to the experimental value than those without the Magnus force. In addition, the energy flux near the ground surface decreased as grain diameter increased, while beyond a specific height, the energy flux increased with grain diameter.

[40] **Acknowledgments.** This research work was supported by grants from the National Key Project for Basic Research (2009CB421304) and the National Natural Science Foundation of China (10811130470, 10772073). The authors sincerely appreciate this support. The authors also thank the anonymous reviewers and editors for their thoughtful comments which helped to improve and clarify the paper.

References

Anderson, R. S., and P. K. Haff (1988), Simulation of aeolian saltation, *Science*, *241*, 820–823, doi:10.1126/science.241.4867.820.

Anderson, R. S., and B. Hallet (1986), Erosion profiles due to particles entrained by wind: Application of an eolian sediment-transport model, *Geol. Soc. Am. Bull.*, *97*, 1270–1278, doi:10.1130/0016-7606(1986)97<1270:EPDTPE>2.0.CO;2.

Anderson, R. S., C. Santa, M. A. Sorenson, and B. B. Willetts (1991a), A review of recent progress in our understanding of aeolian sediment transport, *Acta Mech.*, *1*, Suppl., 1–19.

Anderson, R. S., C. Santa, and P. K. Haff (1991b), Wind modification and bed response during saltation of sand in air, *Acta Mech.*, *1*, Suppl., 21–25.

Bagnold, R. A. (1941), *The Physics of Blown Sand and Desert Dunes*, Methuen, New York.

Bo, T., L. Xie, and X. J. Zheng (2007), Simulation of wind ripples, *Int. J. Nonlinear Sci. Numer. Simul.*, *7*, 223–228.

Chepil, W. S., and N. P. Woodruff (1963), The physics of wind erosion and its control, *Adv. Agron.*, *15*, 211–302, doi:10.1016/S0065-2113(08)60400-9.

Gillette, D. A., and P. H. Stockton (1986), Mass momentum and kinetic energy fluxes of saltating particles, in *Aeolian Geomorphology*, edited by W. G. Nickling, pp. 35–56, Allen and Unwin, London.

Huang, N., and X. J. Zheng (2003), Effects of wind-blown sand movement and Magnus force on effective roughness (in Chinese, with English abstract), *J. Desert Res.*, *23*, 616–620.

Huang, N., X. J. Zheng, Y. H. Zhou, and S. V. Pelt (2006), Simulation of wind-blown sand movement and probability density function of liftoff velocities of sand particles, *J. Geophys. Res.*, *111*, D20201, doi:10.1029/2005JD006559.

Kok, J. F., and N. O. Renno (2008), Electrostatics in wind-blown sand, *Phys. Rev. Lett.*, *100*(1), 014501, doi:10.1103/PhysRevLett.100.014501.

Kok, J. F., and N. O. Renno (2009), A comprehensive numerical model of steady-state saltation, *J. Geophys. Res.*, *114*, D17204, doi:10.1029/2009JD011702.

Owen, P. R. (1964), Saltation of uniform grains in air, *J. Fluid Mech.*, *20*, 225–242, doi:10.1017/S0022112064001173.

Rasmussen, K. R., and M. Sorensen (2008), Vertical variation of particle speed and flux density in aeolian saltation: Measurement and modeling, *J. Geophys. Res.*, *113*, F02S12, doi:10.1029/2007JF000774.

Shao, Y. P. (2000), *Physics and Modelling of Wind Erosion*, Kluwer Acad., Dordrecht, Netherlands.

Ungar, J. E., and P. K. Haff (1987), Steady state saltation in air, *Sedimentology*, *34*, 289–299, doi:10.1111/j.1365-3091.1987.tb00778.x.

Werner, B. T. (1990), A steady-state model of wind-blown sand transport, *J. Geol.*, *98*, 1–17, doi:10.1086/629371.

White, B. R., and J. C. Schultz (1977), Magnus effect in saltation, *J. Fluid Mech.*, *81*, 497–512, doi:10.1017/S0022112077002183.

Zheng, X. J., L. Xie, and X. Y. Zou (2006), Theoretical prediction of liftoff angular velocity distributions of sand particles in wind-blown sand flux, *J. Geophys. Res.*, *111*, D11109, doi:10.1029/2005JD006164.

Zhou, Y. H., X. Guo, and X. J. Zheng (2002), Experimental measurement of wind-sand flux and sand transport for naturally mixed sands, *Phys. Rev. E*, *66*, 021305-1–02305-9.

Zou, X. Y., Z. L. Wang, and Q. Z. Hao (2001), The distribution of velocity and energy of saltating sand grains in a wind tunnel, *Geomorphology*, *36*, 155–165, doi:10.1016/S0169-555X(00)00038-6.

Zou, X. Y., H. Cheng, C. L. Zhang, and Y. Z. Zao (2007), Effects of the Magnus and Saffman forces on the saltation trajectories of sand grain, *Geomorphology*, *90*, 11–22, doi:10.1016/j.geomorph.2007.01.006.

N. Huang, X. Pan, and C. Wang, Key Laboratory of Mechanics on Disaster and Environment in Western China, Ministry of Education, Department of Mechanics, Lanzhou University, Lanzhou 730000, China. (huangn@lzu.edu.cn)